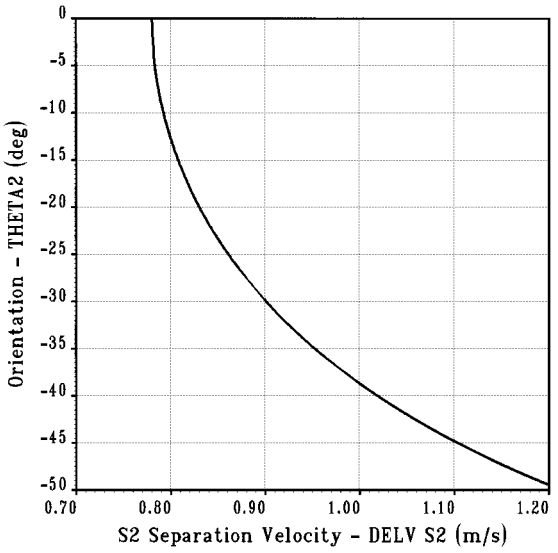

Fig. 1 Separation conditions of S_2 for collision with S_1.

the range (−23.0 deg, 23.0 deg) or $|\theta_2| > 35$ deg to avoid an S_1-S_2 close-contact possibility. Note again that arriving at these conclusions through MC analysis is computationally demanding and time consuming because many combinations have to be tried in which a large number of simulations (orbit propagation) for each of the combinations is carried out.

Although the strategy is demonstrated in the case of two satellites, it can be used[5] even when there are more satellites to find deployment conditions for each satellite to avoid a close-contact possibility among all of them. A system of separation springs for satellites can be designed to meet the noncollision separation velocity taking into account the masses. Also, orientation can be planned through proper control strategies. The orientation angle leading to recontact of P and S_1 and P and S_2 can also be computed using this strategy. For this example, no angle leads to such a recontact possibility between P and S_1 and an angle of approximately 90 deg leads to the collision of P and S_2.

Conclusions

A strategy to arrive at separation velocity and its orientation with respect to instantaneous velocity, for the deployment of a satellite such that it avoids collision with another satellite in orbit within one revolution, deployed either simultaneously or a short time earlier, has been presented. Efficiency of the strategy under various force models and variations in the time gap between the deployments of the satellites has been analyzed. This strategy enables postinjection operations on satellites to put them into the proper location without the risk of collision. The fuel onboard, generally carried to account for collision risk, can be saved.

Acknowledgments

The author expresses his sincere thanks to reviewers for their comments and observations. He wishes to express his gratitude to V. Adimurthy, Shri Madanlal, Shri K. Kumar, and P. V. Subba Rao, for their encouragement and for technical discussions.

References

[1]Yarbrough, P. G., "Operation Concept for the World's First Commercially Licensed Low-Earth Orbiting Mobile Satellite Service," AIAA Paper 96-1049-CP, Feb. 1996.

[2]Spagnulo, M., and Sabathier, V., "An Ariane Strategy for In-Orbit Separation of Satellite Constellations," *Proceedings of the 46th International Astronautical Congress*, International Astronautical Federation, IAF-95-A.6.06, 1995.

[3]Brown, C. D., *Spacecraft Mission Design*, AIAA Education Series, AIAA, Washington, DC, 1992, p. 14.

[4]Escobal, P. R., *Methods of Orbit Determination*, Wiley, New York, 1965, p. 397.

[5]Ramanan, R. V., "On the Collision Possibility of Satellites Deployed by a Single Vehicle During First Revolution," VSSC-APMD-TM-PSLV-017-1998.

Minimization of Vibration of Spacecraft Appendages During Shape Control Using Smart Structures

Serdar Kalaycioglu* and David Silva†
Canadian Space Agency,
St. Hubert, Quebec J3Y 8Y9, Canada

I. Introduction

LARGE space structures are inherently flexible, and this property tends to slow down, while increasing the cost of critical space maneuvers such as space station remote manipulator system positioning, and the deployment and orientation of solar panels, antennas, etc. The advent of smart structures is perceived as a promising alternative for the implementation of improved sensing and active control of vibration and shape for the next generation of large flexible space structures, such as space stations. Although there exist many alternatives to develop smart structures that can be used to implement the different modern shape control approaches, we concentrate on the use of PZTs. The modeling of the induced-strain actuation produced by these devices can be found in the work of Crawley and Anderson.[1]

In this Note, a dynamic model, originally developed in a flexible appendage deployment context,[2] is extended to include a smart structure and is used to minimize the vibrational motion of an elastic cantilevered plate with a glued collocated sensor/actuator pair of fiber-optic strain sensor and piezoceramic actuator (PZT), during the application of a static shape control scheme.

The process of shape control based on smart structures estimates the target voltage values for the PZT actuators to correct the deformed shape of an appendage. However, the voltage profiles, that is, variation of voltage with respect to time, for each actuator may not be obtained because the shape control process provides only the initial and final static voltage values. After direct application of these voltages, via the PZT actuators, a successful shape correction of the appendage can be realized. Nevertheless, the arbitrary selection of any admissible control voltage profile leading from the initial voltage values to the final voltage values causes transient and residual vibrations.

The optimum voltage profile is obtained using Pontryagin's principle for the variation of the PZT voltages, under the restriction of minimum vibrational motion during the shape correction process. The resulting two-point boundary problem is solved using a multiple-shooting algorithm to obtain the desired optimum solution. The optimum solution is exhibited, experimentally tested, and compared with other admissible control profiles.

II. Dynamic Model of the Smart Structure

The flexible appendage of a spacecraft is characterized by means of a plate with some glued or embedded piezoceramic actuators and fiber-optic strain sensors. An example of the geometry of such a system is shown in Fig. 1.

In Fig. 1, A_0, B_0, and H_0 represent the physical dimensions of the plate, whereas A_i, B_i, and H_i are those of the PZT actuators, with $i = 1, \ldots, m$, where m is the number of actuators. In Fig. 1, the coordinate axes are represented by x, y, and z.

Let the instantaneous transverse elastic displacement along the z axis be $w(x, y, t)$. For the convenience of the analysis we assume that w is separable into its temporal and spatial components, and

Received 15 May 1997; revision received 14 September 1999; accepted for publication 8 November 1999.

*Manager, Strategic Automation and Robotics Technologies, 6767 Airport Road; serdar.kalaycioglu@space.gc.ca.

†Student Employee, Space Technologies Branch; currently Engineer, CAE Electronics, 8585 Cote de Liesse, Saint-Laurent, Quebec, Canada H4T 1G6.

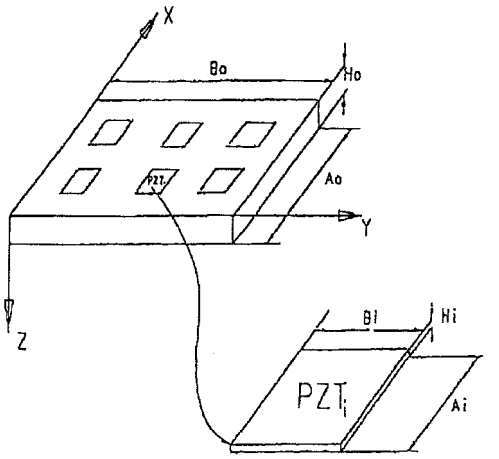

Fig. 1 Geometry of the plate and the PZT actuators.

we further assume the existence of a complete set of functions that allows w to be expanded in series as follows:

$$w(x, y, t) = \sum_{s=1}^{ns} \sum_{r=1}^{ms} W_{rs}(t)\phi_r(x)\psi_s(y) = \boldsymbol{\Phi}^T \boldsymbol{W} \boldsymbol{\Psi} \tag{1}$$

Furthermore,

$$\boldsymbol{w}(x, y, t) = \boldsymbol{C}_{\Phi\Psi}^T \tilde{W}$$

where

$$\boldsymbol{C}_{\Phi\Psi}^T = [\phi_1\psi_1 \;\; \phi_1\psi_2 \;\; \cdots \;\; \phi_1\psi_n \;\; \phi_2\psi_1 \;\; \phi_2\psi_2 \;\; \cdots \;\; \phi_2\psi_n \;\; \cdots \;\; \phi_m\psi_n] \tag{2}$$

$$\tilde{\boldsymbol{W}}^T = [W_{11} \;\; W_{12} \;\; \cdots \;\; W_{1n} \;\; W_{21} \;\; W_{22} \;\; \cdots \;\; W_{2n} \;\; W_{31} \;\; \cdots \;\; W_{mn}] \tag{3}$$

If the functions $\phi_r(x)$ and $\psi_s(y)$ satisfy the kinematic boundary conditions of the plate and form a complete set, then the series will converge to the true solution in the limit as $ms, ns \to \infty$. Nevertheless, by a judicious choice of the sets $\{\phi_r(x)\}$ and $\{\psi_s(y)\}$ it is often possible to obtain very good approximations to the true solution by taking only the first few terms of the series. In fact, for the shape functions, the eigenfunctions of a free–free and clamped–free (cantilever) beam can be used to advantage. These functions are not only complete, but they satisfy all of the boundary conditions.

To apply the Lagrangian formalism, we use $\tilde{W}_{ij}$ and $\dot{\tilde{W}}_{ij}$ as our generalized coordinates in the expressions for the kinetic and potential energy. By carrying out some algebraic manipulations, one obtains the equations of motion,

$$\boldsymbol{M}\ddot{\tilde{\boldsymbol{W}}} + \boldsymbol{D}_w \dot{\tilde{\boldsymbol{W}}} + \boldsymbol{K}\tilde{\boldsymbol{W}} = \tilde{\boldsymbol{F}} \tag{4}$$

which govern the vibrations of the plate. $\boldsymbol{D}_w$ is the damping matrix and is assumed to be diagonal. The matrix $\boldsymbol{M}$ is the mass matrix and is equal to $a_0 b_0 \mathbf{1}$ [where $\mathbf{1}$ is a unity matrix of size $(nsms \times nsms)$]. $\tilde{\boldsymbol{F}}$ is the generalized forces due to the piezoceramics actuator control forces $\tilde{\boldsymbol{F}}_c$ and the external disturbances $\tilde{\boldsymbol{F}}_d$:

$$\tilde{\boldsymbol{F}} = \tilde{\boldsymbol{F}}_c + \tilde{\boldsymbol{F}}_d \tag{5}$$

In the following, the contribution of the external forces $\tilde{\boldsymbol{F}}_d$ is assumed to be null. The equivalent generalized force due to the PZTs can be calculated as follows:

$$\tilde{\boldsymbol{F}}_c = \boldsymbol{M}\ddot{\tilde{\boldsymbol{W}}}_{mij} + \boldsymbol{D}_w \dot{\tilde{\boldsymbol{W}}}_{mij} + \boldsymbol{K}\tilde{\boldsymbol{W}}_{mij} \tag{6}$$

$$\tilde{\boldsymbol{F}}_c = \boldsymbol{M}\boldsymbol{Q}\ddot{\tilde{\boldsymbol{V}}}(t) + \boldsymbol{D}_w \boldsymbol{Q}\dot{\tilde{\boldsymbol{V}}}(t) + \boldsymbol{K}\boldsymbol{Q}\tilde{\boldsymbol{V}}(t) \tag{7}$$

where $\boldsymbol{Q}$ is a matrix [of size $(ns \times ms) \times m$] composed of $\tilde{q}_i$, where m is the number of actuators and ns and ms are the number of modes taken into account in F–F and C–F eigenfunctions, respectively. Thus,

$$\boldsymbol{Q} = [\tilde{\boldsymbol{q}}_1 \;\; \tilde{\boldsymbol{q}}_2 \;\; \cdots \;\; \tilde{\boldsymbol{q}}_m] \tag{8}$$

The vector $\tilde{\boldsymbol{V}}$ is the applied actuating voltage profile and $\tilde{\boldsymbol{q}}_i$ is a constant vector for each PZT. The details of the derivation of the generalized forces due to the PZTs are given elsewhere.[3]

The developed shape control algorithm determines the target voltage values necessary to correct the deformed geometry for each of the deformed PZT actuators in the system. Therefore, the initial voltage values $\tilde{V}_0$ will be increased to $\tilde{V}_f$ within a time interval $[0, t_f]$. Applying the methods of the calculus of variations, we impose the minimization of vibrations during the shape correction maneuver by minimizing the objective function

$$J = \int_0^{t_f} \int_0^1 \int_0^1 u^2 \, \mathrm{d}\eta \, \mathrm{d}\zeta \, \mathrm{d}t \tag{9}$$

where $u = [w(\eta, \zeta, t), \dot{w}(\eta, \zeta, t)]$. After substituting the discretized deformation and integrating around the area, one obtains J as

$$J = \int_0^{t_f} [\tilde{W}^T \tilde{W} + \dot{\tilde{W}}^T \dot{\tilde{W}}] \, \mathrm{d}t \tag{10}$$

The given objective function J is subject to the constraints represented by the equations of motion. It is convenient to introduce a new variable η_0 characterized by

$$\dot{\eta}_0 = \tilde{W}^T \tilde{W} + \dot{\tilde{W}}^T \dot{\tilde{W}} = g_0 \tag{11}$$

$$\phi_0 = \dot{\eta}_0 - g_0 = 0 \tag{12}$$

The second-order structural equations of motion can be written in the state-space form as

$$\phi_i = \dot{\eta}_i - g_i = 0 \tag{13}$$

where the η_i are the state variables consisting of the generalized coordinates W_i and W_i. Next, one formulates the function G defined by

$$G(\lambda_i, \dot{\lambda}_i, \eta_i, \dot{\eta}_i, \tilde{V}, \dot{\tilde{V}}, \ddot{\tilde{V}}) = \sum_{i=0}^{k} \lambda_i \phi_i \tag{14}$$

$$G(\lambda_i, \dot{\lambda}_i, \eta_i, \dot{\eta}_i, \tilde{V}, \dot{\tilde{V}}, \ddot{\tilde{V}}) = \sum_{i=0}^{k} \lambda_i [\dot{\eta}_i - g_i] \tag{15}$$

where the λ_i are a set of Lagrange multipliers and k is the total number of modes taken into account.

After performing the variations one obtains a set of nonlinear equations, whose solution give the optimal voltage variations for each of the m PZT actuators that govern the vibrations of the flexible structure,

$$\lambda_i \left(\frac{\partial g_i}{\partial \eta_i} - \frac{\mathrm{d}}{\mathrm{d}t}\left[\frac{\partial g_i}{\partial \dot{\eta}_i} \right] \right) + \dot{\lambda}_i \left[1 - \frac{\partial g_i}{\partial \dot{\eta}_i} \right] = 0, \qquad i = 1, 2, \ldots, k \tag{16}$$

$$\dot{\eta}_i - g_i = 0, \qquad i = 1, 2, \ldots, k \tag{17}$$

$$\lambda_i \left(\frac{\partial g_i}{\partial \tilde{V}} - \frac{\mathrm{d}}{\mathrm{d}t}\left[\frac{\partial g_i}{\partial \dot{\tilde{V}}} \right] \right) - \dot{\lambda}_i \frac{\partial g_i}{\partial \dot{\tilde{V}}} = 0, \qquad i = 1, 2, \ldots, k \tag{18}$$

Note that some of the boundary conditions are at $t = 0$, whereas the others are at $t = t_f$. The set of equations along with the boundary conditions constitute a nonlinear two-point boundary-value problem. This can be solved only numerically; in this work this was done using a multiple-shooting method.

III. Simulation and Experimental Results

The experimental setup (Fig. 2) consists of a cantilever aluminum beam with a glued collocated sensor/actuator pair consisting of a fiber-optic strain sensor and a PZT actuator under real-time control using an A/D–D/A card and a controlled voltage power supply that drives the PZT actuator. Technical specifications of the instrumentation used are given in Table 1. Figure 3 shows the placement of the collocated actuator/sensor pair on the cantilever beam.

Table 1 Instrumentation specifications

Instrument	Specification
PZT actuator	Piezo Systems, type PSI-5A-ENH PZT, thickness 0.0075 in., $d_{31} = -190 \times 10^{-12}$ m/V
Strain sensor	Fiso Technologies, Fabry–Perot type, range +2000 μstrain, accuracy 0.01%
Power supply	Kepco, bipolar controlled power supply, +500 V
A/D card	Data Translation, DT16-EZ board with 16-bit resolution

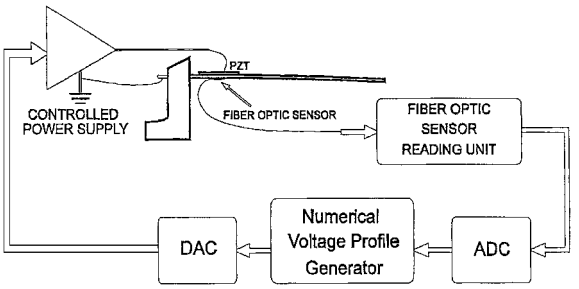

Fig. 2 Schematic of the experimental setup.

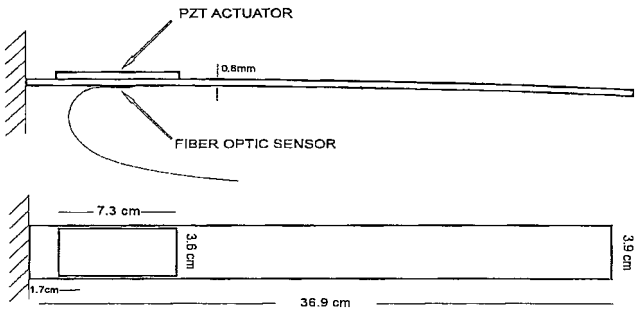

Fig. 3 Location of the actuator/sensor pair.

Superiority of the obtained optimal voltage profile can be appreciated only when it is compared with other profiles. Hence, several simple profiles are considered, and their corresponding vibratory responses are determined for the beam-type flexible structure. These are compared subsequently with the optimal solution.

In each case, the voltages for the PZT actuators vary from $\tilde{V}_0$ to $\tilde{V}_f$ within a time duration of t_f milliseconds.

The simple voltage profiles used with Eq. (7) are

$$\tilde{V} = \tilde{V}_0 + t\tilde{a}, \qquad \tilde{a} = (\tilde{V}_f - \tilde{V}_0)/t_f$$

which represents a ramp profile with a rate of $\tilde{a}$,

$$V_j = b_j + c_j \exp(t), \qquad b_j = \left[\frac{V_{0j}\exp(t_f) - V_{fj}}{\exp(t_f) - 1}\right]$$

$$c_j = \frac{V_{fj} - V_{0j}}{\exp(t_f) - 1}$$

which is called the exponential profile, and

$$\tilde{V} = \tilde{V}_0 + \tilde{c}\sin(kt), \qquad \tilde{c} = \tilde{V}_f - \tilde{V}_0, \qquad k = \pi/2t_f$$

which is identified as the sinusoidal profile.

Figure 4 shows the variations of the voltage profiles $\tilde{V}$ for the PZT actuators glued on the surface of the plate, during the 100 ms to reach steady-state values estimated for the static shape control.

Computer simulation results are obtained for the flexible plate-type structure with PZT actuators. The maximum voltage of 250 V is attained by the applied voltage profiles within $t_f = 100$ ms. The response to these actuating voltages, in terms of μstrain, is shown in Fig. 5.

Figure 6 presents the experimental measured strain caused on the structure by the actuating voltage profiles, applied during the 100 ms to reach the maximum input voltage for the static shape control.

Table 2 Maximum strain values in θ strain units

t_f, to reach maximum value, ms	Ramp	Exponential	Sinusoidal	Optimum
250	0.3223	0.2439	0.2101	0.1487
200	0.2376	0.2474	0.2818	0.1487
125	0.4305	0.5104	0.5543	0.1487
100	0.5862	0.7131	0.7676	0.1487

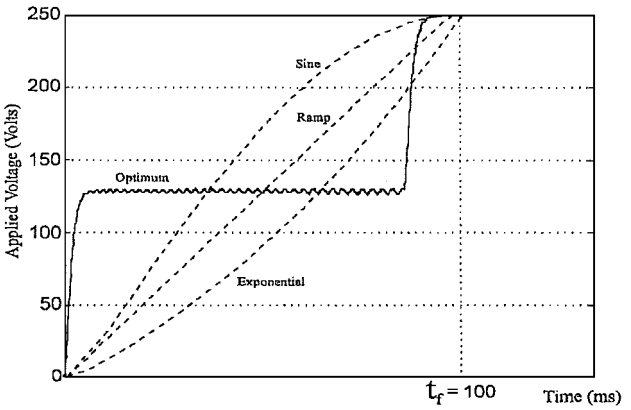

Fig. 4 Applied voltage profiles.

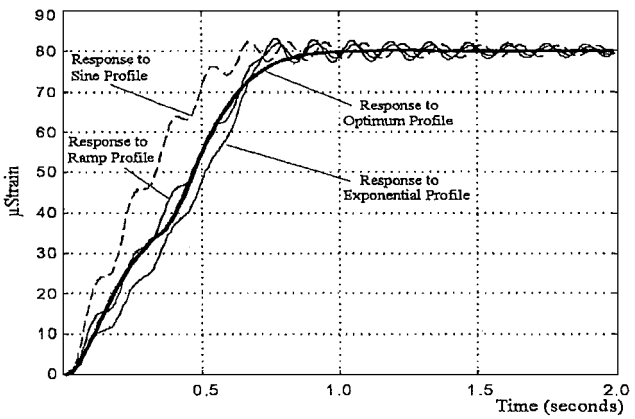

Fig. 5 Computer simulations results.

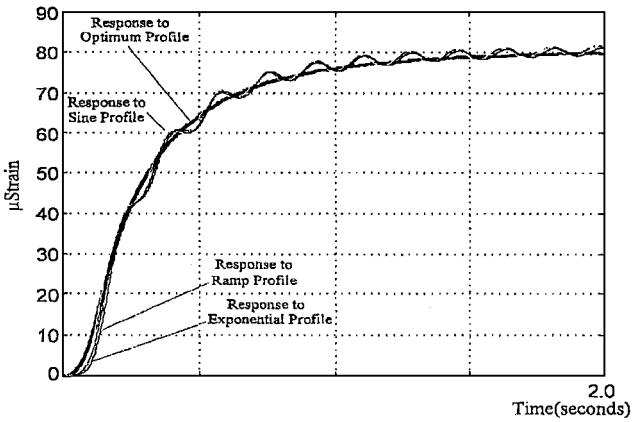

Fig. 6 Experimental results of the strain responses.

The maximum experimental strain measurements acquired by the fiber-optic strain sensor located close to the tip of the appendage are listed in Table 2.

The optimum profile provided vibrations with the smallest amplitude among the overall profiles and the effectiveness of the optimum scheme become even more apparent during quick maneuvers, that is, for smaller t_f. In all other schemes, that is, ramp, exponential, and sinusoidal, the larger values of strain and vibration amplitude

are observed during the faster process of shape corrections, that is, for smaller t_f.

IV. Conclusions

A novel mathematical model, computer simulations, and experimental verifications of minimum vibrations that occur during a static shape control using glued collocated piezoelectric actuator/multichannel fibre-optic sensor pairs is presented. The essence of the approach consists in the application of an optimum voltage profile obtained off-line by use of Pontryagin's principle. The applied optimum voltage profile produced the desired shape modification with negligible vibration of the structure as predicted by the simulation.

The results obtained from the optimum control technique have been compared with those of other admissible control profiles. The experimental and simulation results demonstrated that the developed Pontryagin's principle technique creates minimum transient and residual vibrations and allow faster shape correction maneuvers.

References

[1]Crawley, E. F., and Anderson, E. H., "Detailed Models of Piezoceramic Actuation of Beams," *Journal of Intelligent Materials, Systems, and Structures,* Vol. 1, Jan. 1990, pp. 4–25.

[2]Kalaycioglu, S., and Misra, A., "Approximate Solutions for Vibrations of Deploying Appendages," *Journal of Guidance, Control, and Dynamics*, Vol. 14, No. 2, 1991, pp. 287–293.

[3]Kalaycioglu, S., Giray, M. M., and Asmer, H., "Vibration Control of Flexible Manipulators Using Smart Structures," *Journal of Aerospace Engineering*, ASCE, Vol. 2, No. 3, 1998, pp. 90–94.

Spacecraft Formation Flying: Dynamics and Control

Vikram Kapila*
Polytechnic University, Brooklyn, New York 11201
Andrew G. Sparks†
U.S. Air Force Research Laboratory, Wright–Patterson Air Force Base, Ohio 45433-7521
James M. Buffington‡
Lockheed Martin Tactical Aircraft Systems, Fort Worth, Texas 76101
and
Qiguo Yan§
Polytechnic University, Brooklyn, New York 11201

I. Introduction

A NOVEL concept of distributing the functionality of large spacecraft among smaller, less expensive, cooperative spacecraft is seriously being considered for numerous space missions (see also http://www.vs.afrl.af.mil/factsheets/TechSat21.html).[1] A practical implementation of the concept relies on the control of relative distances and orientations between the participating spacecraft. A ground-based command and control system for relative positioning of multiple spacecraft will be excessively burdened and complex and may not be able to provide sufficiently rapid corrective control commands for formation reconfiguration and collision avoidance. Thus, the concept of autonomous formation flying of spacecraft clusters is vigorously being studied by numerous researchers. In particular, NASA and the U.S. Air Force have identified multiple spacecraft formation flying (MSFF) as an enabling technology for future missions. NASA has shown a keen interest in the development of a reliable autonomous formation keeping strategy to deploy multiple spacecraft for deep space missions, e.g., the Earth Orbiter-I and the New Millennium Interferometer (NMI), also known as Deep Space-3. In addition, the U.S. Air Force's TechSat-21 seeks to push the frontier in microscale MSFF to enable global awareness and rapid access to space in the 21st century.

A number of space missions necessitate MSFF. For example, docking of the space shuttle with a space station requires spacecraft rendezvous where it is necessary to fly two spacecraft in close formation in order to capture and dock at the specified time with zero relative velocity. Similarly, spacecraft recovery and servicing missions rely on MSFF. Applications of MSFF to a ground-based terrestrial laser communication system are discussed in Ref. 2, whereas station keeping for the Space Shuttle Orbiter is mentioned in Ref. 3. In recent years Ref. 4 considered MSFF for NASA's NMI, which relies on separated spacecraft interferometry, whereas an MSFF-based stereo imaging concept is discussed in Ref. 5. Finally, in the next millennium the U.S. Air Force's TechSat 21 is expected to provide diverse capabilities, including reconfigurable instantaneous synthetic aperture radar, sensor data fusion from multiple platforms for stereo imaging, theater-wide surveillance, all weather operation and performance, etc., leading to the U.S. Air Force mission of global virtual presence.

Most prior missions requiring MSFF have been carried out using manual flight control[6] and have been limited to one-leader-one-follower configuration. In the case of formation flying of clusters of multiple spacecraft, collision avoidance becomes a significant issue for which ground/manual control may not be reliable. Thus, the development of autonomous formation control strategies is critical to the success of MSFF. Even though the concept of autonomous MSFF has not been flight tested yet, several theoretical and simulation studies dealing with MSFF have been reported in the literature.[2–5,7] In particular, in previous research the nonlinear spacecraft relative position dynamic equations have been developed and linearized[2,8–10] to obtain the Clohessy–Wiltshire (C-W) equations.[9] Furthermore, an impulsive control-based, discrete-time, spacecraft relative position dynamic model and linear quadratic (LQ) regulation technique have been derived in Ref. 2. This methodology has been extended to nonzero set-point tracking control using a combination of feedback and feedforward control techniques.[3] An alternative control scheme using an on-off phase-plane controller can provide ease of implementation. One such algorithm using differential drag elements for actuation is reported in Ref. 11. Latest advances in the phase-plane control design are reported in Ref. 12. Recently, a Lyapunov-based MSFF control design framework has been developed in Ref. 7, which considers absolute attitude alignment and relative translational motion control.

To minimize fuel consumption in MSFF, Refs. 2 and 3 have proposed the use of sample-data, full-state feedback impulsive control schemes. Specifically, a discrete-time model for the linearized spacecraft relative position dynamics has been derived in Ref. 2, assuming that the control is applied impulsively at the sampling instant (as opposed to the standard zero-order, sample-and-hold technique where the control is held constant over the entire sampling interval[13]). However, the approach of Refs. 2 and 3 fails to provide rigorous, a priori guarantees of the closed-loop system stability. This technique also fails to take advantage of recent developments in propulsion technologies. In particular, high-performance Hall thrusters, pulse plasma thrusters, etc., are currently being developed to meet the requirements for future MSFF missions.[14] These low-weight, high-performance thrusters are expected to provide continuous thrusting capabilities for short time intervals, several times every day (if necessary). These advancements in propulsion technologies necessitate the development of novel pulse-based, spacecraft relative position and orientation control laws. In this Note we

Received 29 April 1999; revision received 29 November 1999; accepted for publication 13 January 2000.

*Assistant Professor, Department of Mechanical, Aerospace, and Manufacturing Engineering; vkapila@duke.poly.edu.

†Aerospace Engineer, AFRL/VAAD, 2210 Eighth Street, Suite 21; Andrew.Sparks@va.wpafb.af.mil.

‡Senior Specialist, Flight Control/Vehicle Management Systems, P.O. Box 748; james.m.buffington@lmco.com.

§Graduate Student, Department of Mechanical, Aerospace, and Manufacturing Engineering; qyan01@utopia.poly.edu.